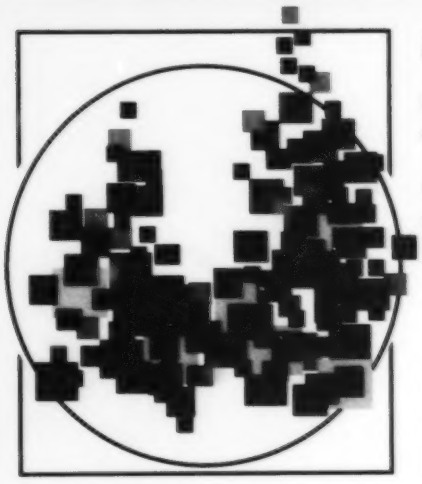

CENTRE FOR
SYSTEMS
SCIENCE

LCCR

Simon Fraser University, Burnaby, B.C., Canada V5A 1S6 / (604) 291-4704

An Adaptive Filtering Technique For Pilot Aided Transmission Systems

Henry Li and J.K. Cavers
CSS/LCCR TR 89-17

December 1989

92-05704/

An Adaptive Filtering Technique For Pilot Aided Transmission Systems

Henry Li and J.K. Cavers

School of Engineering Science
Simon Fraser University
Burnaby, B.C. V5A 1S6
CANADA
Tel: (604) 291-3281

December 1989

ABSTRACT

Many recent papers have revisited the use of pilot tone as a phase and amplitude reference for demodulation on fading channels. The receiver in a pilot aided transmission system extracts the reference with a narrowband pilot filter. Its bandwidth has an optimum value which represents a tradeoff between the amount of distortion and the amount of additive noise present in the Doppler-spread tone. Obviously, the optimum bandwidth varies with vehicle speed. This paper addresses the issue of adjusting the filter bandwidth as speed changes. A novel adaptation technique has been used here, whereby the receiver selects the optimum member from a pre-calculated bank of stored filters. This technique can provide a 1.0 dB improvement for a normalized Doppler frequency of 2% ; up to 2.0 dB can be gained when operating at a lower Doppler frequency. The algorithm is found to be very robust, in the sense that self-noise and decision direction have little effects on its operation and the resulting bit error rate.

This work was funded by the British Columbia Advanced Systems Institute.

I. INTRODUCTION

Recent literature has shown a renewed interest in pilot based calibration systems for combating the effect of multipath fading. The general idea is to transmit a pilot tone along with the data. The receiver then extracts the pilot with a pilot lowpass filter (PF) and the result is used as a phase and/or amplitude reference. One the main advantages of using such a technique is the elimination of the error floor. Some of the disadvantages include non-constant envelope of the resulting signal and the fact that part of the transmitter power needs to be devoted to the pilot. Variations of pilot tone techniques have appeared under different titles such as tone-calibrated technique (TCT) [1], dual-pilot tone calibrated technique (DPTCT) [2] and phase-locked transparent tone in band (PL-TTIB) [3].

One of the main design tradeoffs of pilot based techniques is the pilot filter bandwidth. Ideally, the PF should be just wide enough to accommodate the fade spectrum. This tradeoff has been investigated recently [1]. If it is too narrow, then the filter output cannot follow channel fluctuations. The result is the reappearance of an error floor. If it is too wide, excessive noise will appear in the filter output which can lead to degradation in performance. The optimal bandwidth is one which is just wide enough to cover the fade spectrum. All pilot tone systems proposed to date assume an ideal rectangular PF with bandwidth wide enough to accommodate the worst case Doppler. The actual Doppler frequency during system operation is normally below the expected maximum which means that the PF is too wide most of the time. Figure 1 shows the penalty for using too wide a filter for recovering the pilot. One can observe from this figure that more than 2.0 dB can be gained if the proper PF bandwidth is used at each Doppler frequency (denoted in the figure by f_D). The performance penalty, which is caused by excess additive noise, can be reduced by introducing adaptivity to the PF so that the PF bandwidth may adjust to changes in the Doppler.

There are many adaptive filtering schemes in use today. Most popular are the least mean square (LMS) and recursive least square (RLS) algorithms using either the transversal or lattice structures. Use of the LMS algorithms for PF adaptation has been explored in [5] and the results were found to be discouraging. One of the fundamental drawbacks of these algorithms is the need to update each filter coefficient. In effect, these algorithms all perform multi-dimensional adaptations. However, in the pilot filter application, the

optimum filter for a fixed Doppler frequency is the Wiener filter, which can be shown to be approximately rectangular. An adaptive pilot filter therefore needs only vary its bandwidth, so the adaptation process can be reduced to a single dimension. Our approach to the problem is to store a pre-calculated bank of pilot filters and automatically select the best one as SNR or vehicle speed change. We call this technique the filter switching algorithm (FSA). This paper gives a comprehensive description and analysis of the algorithm.

II. SYSTEM MODEL

The system model used for the analysis of the filter switching algorithm is given in Figure 2. All signals described in this paper are assumed to be in complex envelope representations.

A. Transmitted Signal

The transmitted signal is assumed to be BPSK and Manchester coded to create the spectral null needed for the pilot. This is for simplicity only; the general results do not depend on these assumptions. The transmitted power is split between the data signal s(t), and a pilot having amplitude a. The transmitted complex envelope is given by:

$$z(t) = s(t) + a \tag{1}$$

where the data signal is defined by:

$$s(t) = A \sum_{i=-\infty}^{\infty} b_i \; p(t-iT) \tag{2}$$

p(t) is assumed to be an unit energy pulse such that $\int |p(t)|^2 \, dt = 1$. b_i is the binary data which can assume the values +1 or -1. T is the symbol duration. If we denote the bit rate by R_b and the ratio of pilot tone power to data signal power by r, then:

$$r = \frac{a^2}{A^2 R_b} \tag{3}$$

B. Fading Channel

The pilot-added data signal z(t), is multiplied by a time-varying complex gain g(t) representing the effect of multipath fading. Complex white Gaussian noise $n_s(t)$, with power spectral density N_o, is then added to the modified data signal to form the received signal $r_s(t)$ given by:

$$r_s(t) = g(t)\, z(t) + n_s(t) \tag{4}$$

g(t) is modelled by a zero mean complex Gaussian process with Doppler bandwidth $f_D = v/\lambda$, where v is the vehicle speed and λ is the wavelength of the carrier. Note that we have assumed that the frequency offset between the transmitter and receiver oscillators is made negligible by the use of an accurate AFC. The effect of frequency offset on a tone-aided system using the filter switching algorithm is investigated in [5].

The spectrum of g(t), denoted by S_g, can be written as:

$$S_g(f) = \sigma_g^2 \tilde{S}_g(f) \tag{5}$$

where σ_g^2 is the total power gain and $\tilde{S}_g(f)$ is the fade spectrum normalized to unit power.

The scattering due to multipath reflections is assumed to be isotropic such that the normalized fade spectrum is given by:

$$\tilde{S}_g(f) = \frac{1}{\pi\sqrt{f_D^2 - f^2}} \tag{6}$$

for which the autocorrelation function is:

$$\tilde{R}_g(\tau) = F^{-1}\{\tilde{S}_g(f)\} = J_0(2\pi f_D \tau) \tag{7}$$

$J_0(\cdot)$ is the Bessel function of the first kind with order zero.

C. Received Signal

The received signal is split into two branches, one for the processing of the data signal and the other for the processing of the pilot. At the data branch, the received signal r(t) passes through a unit energy filter which is matched to the modulating pulse shape p(t). The resulting signal is then sampled at rate 1/T. Sampling time is assumed to be in perfect alignment with the bit boundary. Delay is added to the matched filter output in order to

equalize the extra delay incurred at the pilot branch. Assuming that the Doppler frequency is much less than the bit rate, the delayed filter output is given by:

$$u(kT) \approx g(kT)\, A\, b_k + n(kT) \tag{8}$$

n(kT) is additive Gaussian noise with variance N_o.

To obtain a performance reference for the FSA, we remove the data dependence in the delayed matched filter output u(kT) by multiplying it with the demodulated data, $\hat{b}_k$. At low BER, $\hat{b}_k \approx b_k$ so that $\hat{u}(kT)$ can be approximated as:

$$\hat{u}(kT) \approx A\, g(kT) + n_u(kT) \tag{9}$$

where $n_u(kT)$ is Gaussian with variance N_o. Errors introduced by this decision direction are small (see section VI).

The pilot processing branch consists of an integrate and dump filter, a moving window averager (MWA), a bank of reduced coefficient filters and an adaptation loop. The integrate and dump (I & D) filter serves to remove the data modulation present in the received signal. In practice, the I & D filter cannot remove all of the data modulation due to the spectral spreading caused by the channel fading. The result is the presence of data dependent or self-noise in the received pilot. The effect of self-noise has been investigated using simulations in section IV. The sampled I & D filter output is:

$$r_p(kT) = a\, g(kT) + n_p(kT) \tag{10}$$

where $n_p(kT)$ is Gaussian with variance N_o.

The output of the I & D filter is then sampled at rate 1/T and averaged by the MWA having length K. The MWA helps reduce the storage and computational requirements of the algorithm. The reduced coefficient filter determines the shape of the pilot filter impulse response and it has non-zero coefficients spaced by the length of the MWA. We denote the combined impulse response of the MWA and the reduced coefficient filter by $h_p(i, kT)$ where i is the index of the particular filter in the filter bank. Although it is a staircase approximation to the ideal pilot filter, there is little change in performance even for a relatively short MWA. The filter output is:

$$w(kT) = a\,[g(kT) * h_p(i, kT)] + n_w(kT) \tag{11}$$

where * denotes convolution and $n_w(kT)$ is Gaussian with variance KN_o.

w(kT) is conjugated and multiplied by u(t) to form the phase corrected data decision variable d(kT), given by:

$$d(kT) = \mathrm{Re}[u(kT)\, w(kT)^*] \tag{12}$$

The adaptation loop provides the mechanism for selecting the appropriate filter from the filter ensemble. The loop consists of a bank of gradient filters and a sample averager. The gradient filter has an impulse response which equals the difference between the impulse responses of two adjacent reduced coefficient filters. We denote the combined impulse response of the MWA and gradient filter as $\Delta h_p(i,kT)$ as given by:

$$\Delta h_p(i,kT) = h_p(i+1,kT) - h_p(i,kT) \tag{13}$$

The gradient filter output is:

$$v(kT) = a\,[g(kT) * \Delta h_p(i,kT)] + n_v(kT) \tag{14}$$

where $n_v(kT)$ is a noise term with variance $\sigma_{n_v}^2$. v(t) is conjugated and multiplied by the decision corrected data signal $\hat{u}(kT)$ to form an instantaneous cross-correlation y(kT). y(kT) is averaged by a sample averager with length N to produce a sampled cross-correlation:

$$q(kT) = \frac{1}{N}\sum_{m=0}^{N-1} y((m-k)T) = \frac{1}{N}\sum_{m=0}^{N-1} \hat{u}(k-m)\, v(k-m)^* \tag{15}$$

where $(\bullet)^*$ denotes conjugation. The sign of Re[q(kT)] determines the next filter to be used. The control variable Re[q(k)] is denoted by x(kT). A description of the filter operation and the rationale behind the use of x(kT) as control variable is given in the next section. For convenience, sampling period T and filter index i will be omitted from all relevant expressions.

III. FILTER SWITCHING ALGORITHM

A. Filter Operation

The bank of pilot filters consists of filters with different bandwidths from which one is selected for pilot recovery. The filter set is arranged in order of increasing bandwidth. During initial operation, filter with the widest bandwidth is selected and its bandwidth is set to equal to f_{Dmax}. A control variable is then evaluated at some fixed time interval which determines whether to switch to a wider or a narrower filter. After convergence the bandwidth jitters about the optimal value, which equals f_D in the case of rectangular filters. If at a particular time, filter i is selected, it is possible to switch from filter i to filter i+n where i+n is less than or equal to the total number of filters in the set. To simplify analysis, n is restricted to take on values +1 or -1 only.

For the filter switching algorithm, parameters important to the filter operation are filter length and bandwidth spacing. Selection of filter length involves the usual tradeoff between performance, computation complexity and delay. Smaller bandwidth spacing provides some improvement which will be discussed in section V. However, the number of filters and hence the amount of storage space required is inversely proportional to the bandwidth spacing. Moreover, convergence time suffers, since we restricted switches in the algorithm to adjacent filters only.

B. Performance Index Selection

Integral to the design of all adaptive algorithms is the need for a performance index. For the LMS algorithms, mean square error is used. The performance index needs to be well behaved. For the present application, this means that the performance index as a function of the filter bandwidth must not have any local peaks. Since minimum bit error rate (BER) is the ultimate goal, one needs to first examine the various parameters which affect the BER. BER for the transmission of BPSK in a Rayleigh fading channel using pilot tone is a function of the complex correlation coefficient between the matched filter output and the pilot filter output. It is given by [6]:

$$P_e = \frac{1}{2}\left[1 - \sqrt{\rho_r^2/(1-\rho_i^2)}\right] \tag{16}$$

ρ_r and ρ_i are the real and imaginary parts of the complex correlation coefficient ρ where ρ is given by [4]:

$$\rho = \frac{1}{\sqrt{1+(1+r)\frac{N_o}{E_b}}} \frac{\frac{1}{2\pi}\int_{-\pi}^{\pi} \bar{S}_g(e^{j(\omega-\omega o)})\, H_p(e^{j\omega})^*\, d\omega}{\sqrt{\frac{1}{2\pi}\int_{-\pi}^{\pi} \bar{S}_g(e^{j(\omega-\omega o)})\, |H_p(e^{j\omega})|^2\, d\omega + (1+r)\frac{N_o}{E_b}\frac{B_n}{rR_b}}} \tag{17}$$

In (17), $H_p(e^{j\omega})$ denotes the frequency response of the pilot filter having noise bandwidth B_p, and E_b represents the total received energy per bit.

In this paper, we assume that the pilot filter has a real frequency response, i.e. $\rho_i = 0$. For this case, the expression for BER reduces to:

$$P_e = \frac{(1-\rho)}{2} \tag{18}$$

It can be seen from (18) that ρ directly reflects BER. Minimum BER is obtained when ρ is maximized. However, ρ is difficult to compute and analyze. An alternative is to simply use the covariance σ_{uw}^2, which for Rayleigh fading is equivalent to the cross-correlation, since E[u(k)] = E[w(k)] = 0. There are two advantages in using the cross-correlation. Firstly, it easier to compute; there is no need to obtain the variances of the filters output as in the case of correlation coefficients. Secondly, the cross-correlation is linear with respect to the pilot filter response (see eqn. (17)). This means that computing the difference in cross-correlation for two adjacent filters is equivalent to computing the cross-correlation for a filter whose impulse response is the difference in the response of the same two filters. We call this third filter the gradient filter.

We should point out that rectangular filters with identical gain cannot be utilized if cross-correlation is to be used as performance index. This is because the cross-correlations for rectangular filters having the same gain are identical if their bandwidths are greater than f_D, and the switching algorithm will select any of the filters with bandwidths greater than f_D at random. Obviously, only the filter with bandwidth closest to (and greater than) f_D is optimal. In this paper, we assume that the filter is normalized to have unit energy.

Two questior.s remain in determining whether the cross-correlation (denoted as C) is suitable as a performance index. The first question is whether the pilot filter bandwidth corresponding to maximum C, denoted by $B_{p,opt}$, also gives minimum BER or equivalently, whether $B_{p\,opt}$ gives maximum ρ. This can be answered by differentiating C and ρ with respect to the pilot filter bandwidth B_p, setting the derivatives to zero and solving for $B_{p,opt}$. It can be shown that in both cases, $B_{p,opt} = f_D$. The second question is whether ΔC is well-behaved. To answer this, we need to show that C, as a function of B_p, has no local peaks. This can easily be shown to be true by examining the derivative of C with respect to B_p. Detailed analysis of the suitability of C as a performance index can be found in [5].

C. Derivation of the Filter Switching Algorithm

The filter switching algorithm can be summarized as taking a step in a direction opposite to the gradient of C. This is one application of the steepest descent algorithm [7]. The update equation is given by:

$$B_p(n+1) = B_p(n) - \mu \frac{\partial C}{\partial B_p} \tag{19}$$

Approximating $\frac{\partial C}{\partial B_p}$ by $\frac{\Delta C}{\Delta B_p}$ and letting $\mu' = \frac{\mu}{\Delta B_p}$, then:

$$B_p(n+1) = B_p(n) - \mu' \Delta C \tag{20}$$

where ΔB_p represents a step increment in B_p and ΔC represents the resulting change in C. ΔC is given by:

$$\Delta C = E[\hat{u}(k)\, v(k)^*] \tag{21}$$

We now quantize B_p so that only a discrete set of filters is required. To simplify the algorithm further, ΔC is replaced with sign(ΔC). For practical purposes, we approximate the ΔC by a sample mean and use only its real part so that the control variable becomes $x(k) = Re[q(k)]$ where q(k) is defined by (15). The resulting algorithm is then to calculate x(k):

$$\begin{aligned} &\text{If } x(k) > 0, \text{ then } B_p(k+1) = B_p(k) + \Delta B_p \\ &\quad \text{else } B_p(k+1) = B_p(k) - \Delta B_p. \end{aligned} \tag{22}$$

IV. FILTER SWITCHING ANALYSIS

The section provides an analytical model for the filter switching algorithm from which the convergence speed and the average BER can be computed. We first begin with a discussion of some of the assumptions made.

A. Assumptions

In order to simplify analysis, the following are assumed:

1) Adaptation period is equal to the sample size of q(k), N so that values of q(k) used contain no overlapping samples.
2) Values of q(k) taken N samples apart are uncorrelated.
3) There are enough independent samples in q(k) that the sum is Gaussian. Justification for this and the previous assumption lies in the fact that samples in q(k) separated by more than a few fade cycles are essentially uncorrelated.

B. Markov Chain Model

Since the selection of filters depends on x(k), the filter index is a discrete time random variable. Given the three assumptions stated earlier, we can consider successive values of x(k) to be independent. This implies that the filter index i at the next adaptation step depends only on the present value of x(k) and not on any past values of x(k). The process describing i can therefore be represented by a Markov chain. Associated with every Markov chain is a transition probability matrix and an initial state probability vector. For the present application, the transition probabilities are determined by the pdf of x(k). The initial state probability vector has the value one for the highest state M, corresponding to the index of filter with the widest bandwidth, and zero for all others. Given the transition probabilities and the initial state probability vector, a set of steady state probabilities can be computed if the Markov chain is irreducible[1]. For a particular f_D and pilot filter used, BER

---

1 A Markov chain is said to be irreducible if every state can be reached from every other state in a finite number of steps.

can be computed using (17) and (18). The average BER is simply the sum of BER given each filter, weighted by the state probabilities such that:

$$E[P_e] = \sum_{i=1}^{M} \frac{1-\rho(i)}{2} \nu_i \qquad (23)$$

where ν_i denotes the steady state probability for filter i.

An illustration of the Markov chain model described in the previous section is given in Figure 3. In queuing theory, this is the Markov chain of a birth-death process [8] with transitions restricted to one step only. Hence, the transition probabilities are represented by b_i and d_i denoting the birth and death probabilities at state i respectively. As mentioned earlier, in order to obtain the average BER, the steady state probabilities are needed. Unfortunately, the model as shown in Figure 3 is not irreducible since odd and even states alternate. However, the original chain can be split into two, an even and an odd states chain. If we group every two transitions on the original chain into one transition on one of the even or odd state chains, and consider even and odd step transitions separately, then model is identical to that shown in Figure 3. The new model is called dual Markov chain (DMC) model and is illustrated in Figure 4 for the case when M is even. In Figure 4, $p_{i,j}(n)$ denotes the n-step transition probability from state i to state j so that $p_{i,i+1} = b_i$ and $p_{i,i-1} = d_i$.

The transition probability matrices of the DMC model, $\mathbf{P}_{odd}$ and $\mathbf{P}_{even}$ can be obtained from the transition probability matrix of the original chain $\mathbf{P}$ as given by:

$$\mathbf{P}_{odd} = \mathbf{P}_{even} = \mathbf{P}^2 \qquad (24)$$

It can be shown that the even and odd states chains are irreducible so that steady state probabilities exist. Details of the derivation of the steady state probability vector ν for an irreducible Markov chain can be found in [8]. In general, the procedure is to make use of the equation:

$$\nu = [\nu_1, \nu_2, \nu_3, \ldots] = \nu \mathbf{P} \qquad (25)$$

where $$\sum_i \nu_i = 1 \qquad (26)$$

In terms of the state indices of the original chain, the steady state probability vector of the odd states chains can be shown to be given by:

$$v_i = \frac{v_{i-2}\, p_{i-2,i}(2)}{p_{i,i-2}(2)} = \prod_{j=3,odd}^{i} \frac{p_{i-2,i}(2)}{p_{j,j-2}(2)} v_1 \qquad i = 3, 5, \ldots M-1 \qquad (27)$$

where

$$v_1 = \frac{1}{1 + \sum_{i=3,odd}^{M-1} \left\{ \prod_{j=3,odd}^{i} \frac{p_{i-2,i}(2)}{p_{j,j-2}(2)} \right\}} \qquad (28)$$

Similarly, for the even states chain, the steady state probabilities are given by:

$$v_i = \frac{v_{i-2}\, p_{i-2,i}(2)}{p_{i,i-2}(2)} = \prod_{j=4,even}^{i} \frac{p_{i-2,i}(2)}{p_{j,j-2}(2)} v_2 \qquad i = 4, 6, .. M \qquad (29)$$

where

$$v_2 = \frac{1}{1 + \sum_{i=4,even}^{M-1} \left\{ \prod_{j=4,even}^{i} \frac{p_{i-2,i}(2)}{p_{j,j-2}(2)} \right\}} \qquad (30)$$

At any time, the probabilities of having taken an odd or an even number of steps are the same and are equal to 1/2. This means the process on the average spends half its time in the odd state chain and half its time in the even state chain. Consequently, the average steady state probability is simply given by:

$$v_{i,avg} = \frac{1}{2}[v_i] \qquad (31)$$

The transition probabilities b_i are derived from the pdf of x(k) as follows. The adaptation algorithm dictates that if the process is at state i, it will switch to the next higher state if x(k) > 0; otherwise switch to the next lower state. Thus the probability of switch from state i to state i+1 is simply:

$$b_i = p_{i,i+1} = Pr[x(k) > 0] \tag{32}$$

With the Gaussian approximation of x(k), all that are required are the mean and variance of x(k) which are derived next.

C. Statistics of the Sampled Cross-Correlation

Mean

The mean of x(k) is given by:

$$\begin{aligned} E[x(k)] &= E\Big[\frac{1}{N}\sum_{k=0}^{N-1} \mathrm{Re}\,[\hat{u}(k)\, v(k)^*]\Big] \\ &= \frac{1}{N}\sum_{k=0}^{N-1} E\big[\hat{u}_I(k)\, v_I(k) + \hat{u}_Q(k)\, v_Q(k)\big] \\ &= R_{\hat{u}_I v_I}(0) + R_{\hat{u}_Q v_Q}(0) \end{aligned} \tag{33}$$

where $R_{\hat{u}_I v_I}(k)$ and $R_{\hat{u}_Q v_Q}(k)$ are cross-correlation functions between $\hat{u}$ and v as given in Appendix A. E[x(k)] is an important quantity which determines the transition probability. A positive value indicates a net tendency of switching to a higher state (i.e. larger bandwidth).

Variance

The variance of x(k) is given by:

$$\begin{aligned} \mathrm{Var}[x(k)] &= \mathrm{Var}\Big[\frac{1}{N}\sum_{k=0}^{N-1} \mathrm{Re}\,[\hat{u}(k)\, v(k)^*]\Big] \\ &= E\Big[\Big\{\frac{1}{N}\sum_{k=0}^{N-1} \mathrm{Re}\,[\hat{u}(k)\, v(k)^*]\Big\}^2\Big] - \Big\{E\Big[\frac{1}{N}\sum_{k=0}^{N-1} \mathrm{Re}\,[\hat{u}(k)\, v(k)^*]\Big]\Big\}^2 \\ &= E[\{\mathrm{Re}\,[q(k)]\}^2] - \{E[x(k)]\}^2 \end{aligned} \tag{34}$$

$$E[\{\mathrm{Re}\,[q(k)]\}^2] = E\Big[\Big\{\frac{1}{N}\sum_{k=0}^{N-1} \mathrm{Re}\,[\hat{u}(k)\, v(k)^*]\Big\}^2\Big]$$

$$= \frac{1}{N^2} E\Big[\sum_{i=0}^{N-1} \sum_{k=0}^{N-1} \{ \hat{u}_I(i)\, v_I(i)\, \hat{u}_I(k)\, v_I(k) + \hat{u}_I(i)\, v_I(i)\, \hat{u}_Q(k)\, v_Q(k)$$
$$+ \hat{u}_Q(i)\, v_Q(i)\, \hat{u}_I(k)\, v_I(k) + \hat{u}_Q(i)\, v_Q(i)\, \hat{u}_Q(k)\, v_Q(k) \} \Big]$$

Using a result on high order joint moments of Gaussian random variables [9] and after some simple algebraic manipulations, the second moment of x(k) can be shown to be:

$$E[\{\mathrm{Re}\,[q(k)]\}^2] = \frac{2}{N^2} \sum_{i=0}^{N-1} \sum_{k=0}^{N-1} \{ 2\, R_{\hat{u}_I v_I}(0)^2 + R_{\hat{u}_I \hat{u}_I}(i-k)\, R_{v_I v_I}(i-k) + R_{\hat{u}_I v_I}(i-k)^2$$
$$+ R_{\hat{u}_I \hat{u}_Q}(k-i)\, R_{v_I v_Q}(k-i) - R_{\hat{u}_I v_Q}(i-k)^2 \} \qquad (35)$$

(35) can be further simplified by converting the double sums into a single one by using the substitution $l = i-k$. For any function f, it can be shown that:

$$\sum_{i=0}^{N-1} \sum_{k=0}^{N-1} \{ f(i-k) \} = \sum_{l=-(N-1)}^{N-1} \varphi(l)\, f(l) \} \qquad (36)$$

where $\varphi(l) = N - |l|$.

The resulting expression for Var[x(k)] is as follows:

$$\mathrm{Var}[x(k)] = \frac{2}{N^2} \sum_{l=-(N-1)}^{N-1} \{ \varphi(l) \, [2\, R_{\hat{u}_I v_I}(0)^2 + R_{\hat{u}_I \hat{u}_I}(l)\, R_{v_I v_I}(l) + R_{\hat{u}_I v_I}(l)^2$$
$$+ R_{\hat{u}_I \hat{u}_Q}(l)\, R_{v_I v_Q}(l) - R_{\hat{u}_I v_Q}(l)^2] \} - \frac{1}{N} \sum_{k=0}^{N-1} \{ R_{\hat{u}_I v_I}(0) + R_{\hat{u}_Q v_Q}(0) \} \qquad (37)$$

where $\varphi(l) = N - |l|$ as defined previously.

Expressions for the correlation functions $R_{\hat{u}_I \hat{u}_I}(l)$, $R_{v_I v_I}(l)$, $R_{\hat{u}_I \hat{u}_Q}(l)$, $R_{v_I v_Q}(l)$, $R_{\hat{u}_I v_I}(l)$ and $R_{\hat{u}_I v_Q}(l)$ are given in Appendix A.

D. Convergence time

Convergence time of a Markov chain is equivalent to the expected first passage time to the destination state. The method of deriving this convergence time is by first changing the destination state to an absorbing state and renumbering its state index to that of the last state. The transition probability matrix of the modified chain, **P'**, is given by:

$$\mathbf{P'} = \begin{bmatrix} p_{1,1} & \cdots & p_{1,i-1} & p_{1,i+1} & \cdots & p_{1,M} & p_{1,i} \\ p_{2,1} & \cdots & p_{2,i-1} & p_{2,i+1} & \cdots & p_{2,M} & p_{2,i} \\ \vdots & \cdots & \vdots & \vdots & \cdots & \vdots & \vdots \\ p_{i-1,1} & \cdots & p_{i-1,i-1} & p_{i-1,i+1} & \cdots & p_{i-1,M} & p_{i-1,i} \\ p_{i+1,1} & \cdots & p_{i+1,i-1} & p_{i+1,i+1} & \cdots & p_{i+1,M} & p_{i+1,i} \\ \vdots & \cdots & \vdots & \vdots & \cdots & \vdots & \vdots \\ p_{M,1} & \cdots & p_{M,i-1} & p_{M,i+1} & \cdots & p_{M,M} & p_{M,i} \\ 0 & \cdots & 0 & 0 & \cdots & 0 & 1 \end{bmatrix} \tag{38}$$

We can partition **P'** into the following form:

$$\mathbf{P'} = \left[\begin{array}{cccccc:c} p_{1,1} & \cdots & p_{1,i-1} & p_{1,i+1} & \cdots & p_{1,M} & p_{1,i} \\ p_{2,1} & \cdots & p_{2,i-1} & p_{2,i+1} & \cdots & p_{2,M} & p_{2,i} \\ \vdots & \cdots & \vdots & \vdots & \cdots & \vdots & \vdots \\ p_{i-1,1} & \cdots & p_{i-1,i-1} & p_{i-1,i+1} & \cdots & p_{i-1,M} & p_{i-1,i} \\ p_{i+1,1} & \cdots & p_{i+1,i-1} & p_{i+1,i+1} & \cdots & p_{i+1,M} & p_{i+1,i} \\ \vdots & \cdots & \vdots & \vdots & \cdots & \vdots & \vdots \\ p_{M,1} & \cdots & p_{M,i-1} & p_{M,i+1} & \cdots & p_{M,M} & p_{M,i} \\ \hdashline 0 & \cdots & 0 & 0 & \cdots & 0 & 1 \end{array}\right] = \left[\begin{array}{c:c} \mathbf{A} & \mathbf{b} \\ \hdashline \mathbf{0} & 1 \end{array}\right] \tag{39}$$

Let **N** be a matrix defined by:

$$\mathbf{N} = (\mathbf{I} - \mathbf{A})^{-1} \tag{40}$$

with **I** representing the identity matrix with dimension M-1. Furthermore, let $p_k(0)$ denote the initial state probability for state k and $\bar{p}'(0)$ be the row vector with elements:

$$\bar{p}'(n) = [\, p_1(0),\ p_2(0),\ \ldots,\ p_{i-1}(0),\ p_{i+1}(0),\ \ldots,\ p_M(0)\,] \tag{41}$$

It can be shown that **N** exists and that the convergence time (i.e. first passage time) is given by [10]:

$$T_c = \tilde{p}'(0)\, N\, \xi \qquad (42)$$

where ξ is a column vector with all elements being equal to one.

E. Step margin

Because we restrict transitions to one step up or down (no self loops), the filter bandwidth will dither about the optimum value, even when converged. Unfortunately, if the filter bandwidth is too small, the BER will rise sharply [4]. This indicates that some margin of safety should be added to the pilot filter bandwidth chosen. The idea has been incorporated in the filter switching algorithm by selecting pilot filter with bandwidth which is a number of steps wider than that of the filter corresponding to the gradient filter in use. We call this margin of safety (in number of steps) the step margin.

F. Dual Threshold

The algorithm, as presented earlier, forces a switch to a higher or lower bandwidth; there are no self loops in the original Markov Chain. This causes the algorithm to jitter about the optimal state after convergence. One solution is to add a self-loop. To do this, we alter the switching algorithm as follows:

$$\begin{aligned}
&\text{If } x(k) > T1, \\
&\qquad B_p(k+1) = B_p(k) + \Delta B_p \\
&\text{else if } x(k) \le T1 \text{ and } x(k) \le T2, \\
&\qquad B_p(k+1) = B_p(k) \\
&\text{else,} \\
&\qquad B_p(k+1) = B_p(k) - \Delta B_p
\end{aligned} \qquad (43)$$

T1, T2 are transition thresholds. We can see from this new switching algorithm that there is now a finite probability of not changing state and it is equal to $\Pr(T1 \le x(k) \le T2)$. The Markov chain describing the new algorithm is one which represents a pure birth-death process with finite number of states [8]. It can be shown that the new Markov chain is irreducible and the steady state probability vector can be easily computed by solving (25) and (26). The steady state BER follows from (23). It is important to note that the transition thresholds, T1 and T2, need to be made a function of E_b and N_o, since the mean and

variance of the control variable x(k) are functions of E_b and N_o. Although N_o is not expected to change, this means that either E_b or E_b/N_o still needs to be estimated by the algorithm. Unless otherwise specified, however, all results presented will be for the single threshold algorithm.

G. Simulation Results

Monte Carlo simulations were performed to determine the accuracy of the Markov model and to investigate the effects of self-noise and data direction. The fading process was generated by passing white Pseudo-Noise (PN) sequence through an FIR filter whose squared magnitude frequency response approximated the fade spectrum S_g. The AWGN data is represented by another independent PN sequence. Eight samples were used to represent each data bit. The MWA filter was 3 bits long and each reduced coefficient filter had 51 non-zero coefficients (so that the overall pilot filter length is 153). The reduced coefficient filters were optimized for various f_D using Wiener filtering theory at a fixed E_b/N_o of 40 dB. The optimization procedure is discussed in detail in [5].

Figure 5 shows the steady state probabilities from the simulated and computed values for f_D of 2.08% (50 Hz at 2400 bps). Some discrepancies can be noted for filters which are one step wider and one step narrower than the optimum. These have been attributed to the deviation of the sampled cross-correlation pdf from the Gaussian approximation. Note that the filter with the highest steady state probability was the one which has been optimized for 40 Hz Doppler, not 50 Hz, as would be expected if ideal rectangular filters were used. The reason for this will be discussed in the next section. Various parameters were also changed in the simulations including f_D and E_b/N_o in order to determine the effects of self-noise and data direction. In all cases, the effects were found to be negligible.

V. BER PERFORMANCE COMPUTED BASED ON MARKOV MODEL

The effects of various parameters on the BER were investigated. BER curves were computed based on the procedure discussed in section IV. All results were obtained assuming the following unless stated otherwise: ideal rectangular pilot filters, $R_b = 2400$ bps, $r = 0.2$, number of filters = 40, cross-correlation sample size = 300 and bandwidth increment $\Delta B_p = 5$ Hz.

A. General Results Using Ideal Rectangular Pilot Filters

Figure 6 shows the transition probabilities and steady state probabilities for f_D of 100 Hz and E_b/N_o of 20 dB with no step margin. The transition probability depends on the amount of area in the fade spectrum covered by ΔH_p. Because of the shape of the assumed U-shaped fade spectrum, the upward transition probability increases with filter bandwidth, as evident in Figure 6, which indicates an increasing tendency to move up for filters with $B_p < f_D$. Note that the upward transition is nearly zero for $B_p > f_D$. This large tendency to switch to narrower filters is due to the negative gain of the gradient filter response in the range $(-B_p, B_p)$. The steady state probability curve shows an increase as B_p increases to f_D as expected. It should also be noted that the steady state probability had significant values for $B_p \geq 80$ Hz (state 16) and $B_p < 100$ Hz (state 20) which suggests a high error floor .

Convergence time is 21 steps from the last state (largest B_p) and 32 steps from the first state (smallest B_p). Because the transition probabilities are nearly 0 for states with $B_p > f_D$, the process spends almost no time in these states. 32 steps is the worst case convergence time, corresponding to the situation of a vehicle accelerating from standstill to 127 kph (assuming 850 MHz carrier). Recall that one step corresponds to 300 bits of the sample averager, or 125 ms at 2400 bps. Thus, in terms of f_D per second, the average convergence speed is 25 Hz/s. Realistically, the fastest change in f_D which can be expected is only about 15.5 Hz/s (corresponding to at an acceleration of 0-100 kph in 5 seconds). The convergence speed of the filter switching algorithm is, therefore, more than adequate to accommodate any realistic changes in f_D.

One should also note from Figure 6 that because a downward transition probability is nearly one for $B_p > f_D$, tracking is faster for a decrease in f_D than for an increase. Figure 7

shows the average BER vs E_b/N_o. There is an enormous error floor due to transitions into states with too narrow a bandwidth. The optimum power split ratio r was relatively insensitive to changes in E_b/N_o and was found to be 0.33. This is in contrast with the optimum value of 0.2 found for a non-adaptive system in [4]. Varying the number of filters at fixed ΔB_p had little effect on BER performance as long as the bandwidth of the widest filter in the filter set is greater than f_D.

B. Effect of Step Margin

The effect of varying the step margin is shown in Figure 8 for f_D of 50 Hz. As a reference, Figure 8 also shows the BER curve for a non-adaptive system using a rectangular PF with bandwidth of 150 Hz. It can be observed that the irreducible error floor drops as the step margin increases. For a margin of 6, the BER curve is almost parallel to that of the non-adaptive case. The improvement at a BER of 10^{-2} is about 0.8 dB. As will be shown later, the BER improvement is more significant for smaller Doppler. An interesting point worth noting is that as the margin is increased, the low E_b/N_o portion of the BER curve moves upward as a result of increase in the average bandwidth. This indicates a tradeoff between the BER in the low and high E_b/N_o regions when the step margin is varied.

C. Effect of f_D

Figure 9 shows BER for various Doppler spread values, f_D, with a step margin of 5. BER for a lower f_D is smaller than for a higher f_D because the average bandwidth used at lower f_D is smaller. At a BER of 10^{-2}, the improvement over a non-adaptive system is about 2.0 dB for 10 Hz Doppler, 1.0 dB for 50 Hz Doppler and 0.3 dB for 100 Hz Doppler. Note that the error floor is higher for a lower f_D due to the increase in the low frequency component of S_g as f_D is decreased. This indicates that more margin is needed at low f_D.

D. Effect of Bandwidth Increment

Figure 10 shows the BER for two sets of filters with different ΔB_p. Note that different step margins were used so that the margin in frequency remained the same. Performance at low E_b/N_o is about the same for both ΔB_p, but the error floor nearly disappears for the smaller ΔB_p. This is intuitively satisfying because the dc gain of the gradient filter decreases with decreasing ΔB_p. A smaller (negative) dc gain means a higher cross-correlation

which results in larger upward transition probabilities and smaller steady state probabilities for $B_p > f_D$. Since the dc gain has inverse dependence on B_p, the steady state probabilities at smaller B_p are affected more. The overall result is that variations in B_p are less, which means that one can use a smaller step margin and get a corresponding improvement in BER. The cost of using a smaller ΔB_p is the increased storage requirement for more filters.

E. Effect of Cross-Correlation Sample Size

Figure 11 shows the effect of the sample size on the BER for f_D of 100 Hz. The decrease in the sample size is accompanied by a corresponding increase in the error floor. Fewer samples means a shorter time span covering the fading process which leads to greater uncertainty in the cross-correlation estimate. As a result, there is larger spread in the steady state probability and hence a larger error floor. Figure 11 indicates that a minimum of 150 samples are needed in order to keep the error floor low enough. Note that it is the length of the time interval which is important in determining the BER as long as the sampling rate of the fading process is above the Nyquist rate. One could reduce the sample size by increasing the time between samples or by using a longer MWA and obtain a similar BER performance. This is true as long as the reciprocal of the time between samples is greater than the Nyquist rate of the fading process.

F. Dual Threshold

Recall that the use of a single threshold causes jitter in the converged algorithm. We investigated dual thresholds to allow self loops in the Markov chain and therefore to reduce jitter when converged. Figure 12 gives the results of using the dual threshold algorithm for f_D of 100 Hz with various thresholds and no step margin. For simplicity, we set the two thresholds to be constant multiples of E_b/N_o, and they were made symmetrical such that T2 = -T1 where T1 > 0. One striking feature as evident from Figure 12 is the reduction in the error floor as T1 is increased. With thresholds of ± 1.0 E_b/N_o, we can almost do away with step margin. The drastic improvement is due to the increase in the ratios between upward and downward transition probabilities since these ratios determine the steady state probabilities. Increasing the transition thresholds has the effect of decreasing the error floor. Unfortunately, this reduction in error floor also results in a drastic increase in convergence time, as is indicated by Figure 13 which shows the convergence time (in number of steps) as a function of transition threshold (in multiples of E_b/N_o). The increase in con-

vergence time is caused by the increased self-loop probability. In practice, BER performance will also be degraded by noise present in the E_b/N_o estimate.

G. Optimized FIR Filter vs Ideal Rectangular Filters

Ideal rectangular pilot filters were used in all of the results in the previous section. We have also investigated the effect of using FIR filters optimized for various f_D using Wiener filter theory. The investigation showed that a MWA length of 5 and a reduced coefficient filter length of 21 or more should be used. Filter lengths greater than 51 gave no further improvement in performance. A comparison of the BER performance reveals that a smaller step margin is required to maintain a low error floor when using FIR filters. This observation can be explained as follow. A Wiener filter optimized for a particular f_D has a relatively flat frequency response up to f_D, and the response rolls off gradually from there on. This gradual roll-off allows more of the fade spectrum to be covered by the positive gain sections of the gradient filter, when the true Doppler is larger than the value which the filter has been optimized. More spectrum coverage means that the upward transition probabilities are larger and the variations in B_p are smaller. As a result, the amount of step margin required is less. The particular shape of the Wiener filter is also the reason why the steady state probability peaks for a filter which has been optimized for a value lower than the true Doppler.

VI. CONCLUSIONS

Adaptivity in the pilot filter bandwidth can produce a significant improvement in the BER. Our adaptation technique, called the filter switching algorithm, can also be applied to more general situations. A dual Markov chain model was used to analyze the performance of the new algorithm. This model enables the computation of both the average BER and the convergence speed. Simulations showed good agreement between simulated and analytical results based on the DMC model. A comparison of BER performance to a non-adaptive system showed that the improvement provided by the new algorithm is about 0.3 dB improvement for 100 Hz Doppler, 1.0 dB for 50 Hz Doppler and almost 2.0 dB for a 10 Hz Doppler. In addition, the new algorithm is very robust, in the sense that self-noise and decision direction have very little effect on its performance.

APPENDIX A - Derivations of Correlation Functions of $\hat{u}(k)$ and $v(k)$

Due to the limitation of space, only an abbreviated version of the derivations has been presented here. For more details on the derivations, see Appendices 3 and 4 in [5].

In the following derivations, it is assumed that the in-phase and quadrature components of the fading process, g, and the noise process in the decision corrected reference, n_u, are uncorrelated. Furthermore, the autocorrelation functions of their in-phase and quadrature components are assumed to be identical. These assumptions lead to the following:

$$E[g_I(i)\, g_Q(k)] = E[n_{uI}(i)\, n_{uQ}(k)] = 0 \tag{A.1}$$

$$E[g_I(i)\, g_Q(k)] = E[g_I(i)\, g_Q(k)] = R_g(i-k) \tag{A.2}$$

$$E[n_{uI}(i)\, n_{uI}(k)] = E[n_{uQ}(i)\, n_{uQ}(k)] = N_o \tag{A.3}$$

Let $R_{\hat{u}_I\hat{u}_I}(l)$, $R_{\hat{u}_Q\hat{u}_Q}(l)$, $R_{v_Iv_I}(l)$, $R_{v_Qv_Q}(l)$, $R_{\hat{u}_I\hat{u}_Q}(l)$, $R_{v_Iv_Q}(l)$, $R_{\hat{u}_Iv_I}(l)$, $R_{\hat{u}_Iv_Q}(l)$,$R_{\hat{u}_Qv_Q}(l)$ and $R_{\hat{u}_Iv_Q}(l)$ be cross-correlation functions with u_I, u_Q, v_I, v_Q denoting the in-phase and quadrature components of $\hat{u}$ and v respectively. It is trivial to show that $R_{\hat{u}_I\hat{u}_Q}(l)$, $R_{\hat{u}_Iv_Q}(l)$, $R_{v_Iv_Q}(l)$ and $R_{\hat{u}_Iv_Q}(l)$ equal zero since R_g and h_p are real. The remaining terms are obtained as follows.

$$\begin{aligned} R_{\hat{u}_I\hat{u}_I}(i-k) &= E[\hat{u}_I(i)\, \hat{u}_I(k)] \\ &= E[\{A\, g_I(i) + n_{uI}(i)\}\{A\, g_I(k) + n_{uI}(k)\}] \\ &= E[g_I(i)\, g_I(k)]\, A^2 + E[n_{uI}(i)\, n_{uI}(k)] \\ &= \frac{E_b}{1+r} R_g(i-k) + \sigma_{n_u}^2 \delta_{ik} \end{aligned} \tag{A.4}$$

where (3), (9), (A.1), (A.2) and (A.3) were used.

$$\begin{aligned} R_{v_Iv_I}(i-k) &= E[v_I(i)\, v_I(k)] \\ &= E\Big[\{a\, \mathrm{Re}[g(i) * \Delta h_p(i)] + n_{vI}(i)\}\ \{a\, \mathrm{Re}[g(k) * \Delta h_p(k)] + n_{vI}(k)\}\Big] \\ &= E\Big[\Big\{a \sum_{n=-\infty}^{\infty} \{g_I(i-n)\, \Delta h_p(n) + n_{vI}(i)\}\Big\}\Big\{a \sum_{m=-\infty}^{\infty} \{g_I(k-m)\, \Delta h_p(m)\} + n_{vI}(k)\Big\}\Big] \\ &= a^2 \sum_{n=-\infty}^{\infty} \sum_{m=-\infty}^{\infty} \{E[g_I(i-n)\, g_I(k-m)]\, \Delta h_p(n)\, \Delta h_p(m)\} + E[n_{vI}(i)\, n_{vI}(k)] \end{aligned}$$

$$= \frac{r}{1+r} E_b R_b \sum_{n=-\infty}^{\infty} \sum_{m=-\infty}^{\infty} \left\{ \tilde{R}_g(i-n-(k-m)) \, \Delta h_p(n) \, \Delta h_p(m) \right\} + \sigma_{n_v}^2 \, \delta_{ik} \qquad \text{(A.5)}$$

where (3), (14), (A.1) and (A.2) were used. $\sigma_{n_v}^2$ is the noise variance at the gradient filter output given by:

$$\sigma_{n_v}^2 = \frac{N_0}{2\pi} \int_{-\pi}^{\pi} |\Delta H_p(e^{j\omega})|^2 \, d\omega \qquad \text{(A.6)}$$

$$\begin{aligned} R_{\hat{u}_I v_I}(i-k) &= E[\hat{u}_I(i) \, v_I(k)] \\ &= E\left[\left\{ A\{g_I(i) + n_{u_I}(i)\} \right\} \left\{ a \sum_{m=-\infty}^{\infty} \left\{ g_I(k-m) \, \Delta h_p(m) \right\} + n_{v_I}(k) \right\} \right] \\ &= a \, A \sum_{n=-\infty}^{\infty} \left\{ E[\, g_I(i) \, g_I(k-n)] \, \Delta h_p(n) \right\} \\ &= E_b \frac{\sqrt{r R_b}}{1+r} \sum_{n=-\infty}^{\infty} \left\{ \tilde{R}_g(i-(k-n)) \, \Delta h_p(n) \right\} \end{aligned} \qquad \text{(A.7)}$$

where (3), (9), (14), (A.1) and (A.2) were used.

Similar analysis can be performed for the remaining terms so that the following can be shown to be true:

$$R_{\hat{u}_Q \hat{u}_Q}(i-k) = R_{\hat{u}_I \hat{u}_I}(i-k) \qquad \text{(A.8)}$$

$$R_{v_Q v_Q}(i-k) = R_{v_I v_I}(i-k) \qquad \text{(A.9)}$$

$$R_{\hat{u}_Q v_Q}(i-k) = R_{\hat{u}_I v_I}(i-k) \qquad \text{(A.10)}$$

REFERENCES

1. Faramaz Davarian, "Mobile Digital Communication via Tone Calibration," IEEE Trans. on Veh. Technol., Vol. VT-36, No. 2, pp. 55-62, May 1987.

2. M. K. Simon, "Dual-Pilot Tone Calibration Technique," IEEE Trans. on Veh. Technol., Vol. VT-35, No. 2, pp. 63-70, May 1986.

3. J. P. McGeehan, A. J. Bateman, "Phase-Locked Transparent Tone-in-Band (TTIB): A New Spectrum Configuration Particularly Suited to the Transmission of Data Over SSB Mobile Radio Networks," IEEE Trans. on Comm. Vol. COM-32, No. 1, pp. 81-87, Jan. 1984.

4. J. K. Cavers, "Performance of Tone Calibration With Frequency Offset and Imperfect Pilot Filter," Technical Report: CSS/LCCR TR 88-15, Center for Systems Science, Simon Fraser University.

5. H. Li, "Adaptive Filtering Techniques for Tone Aided Transmission System," M.A.Sc. Thesis, Simon Fraser University, Feb. 1990.

6. J. G. Proakis, *Digital Communications*, McGraw-Hill, 1983.

7. B. Widrow, S. D. Stearns, *Adaptive Signal Processing* , Prentice-Hall, 1985.

8. K. S. Trivedi, *Probability and Statistics with Reliability, Queueing, and Computer Science Applications*, Prentice-Hall, 1982.

9. J. M. Wozencraft and I. M. Jacobs, *Principles of Communication Engineering*, Wiley, 1965.

10. J. G. Kemeny and J. L. Snell, *Finite Markov Chains*, D. Van Nostrand Company Ltd., 1960.

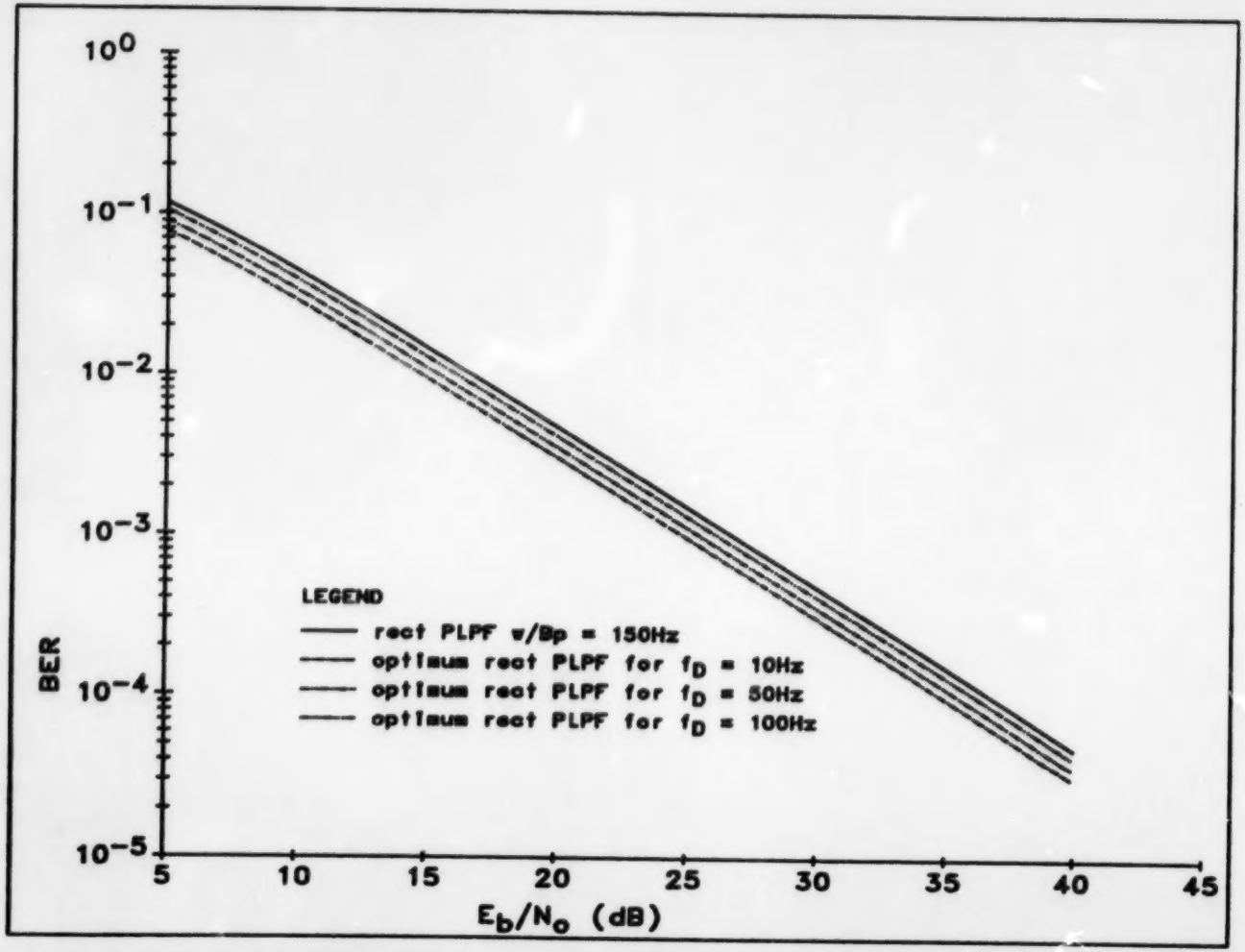

Figure 1 - Performance Penalty for Using a Non-Adaptive Pilot Filter with a Bandwidth of 150Hz

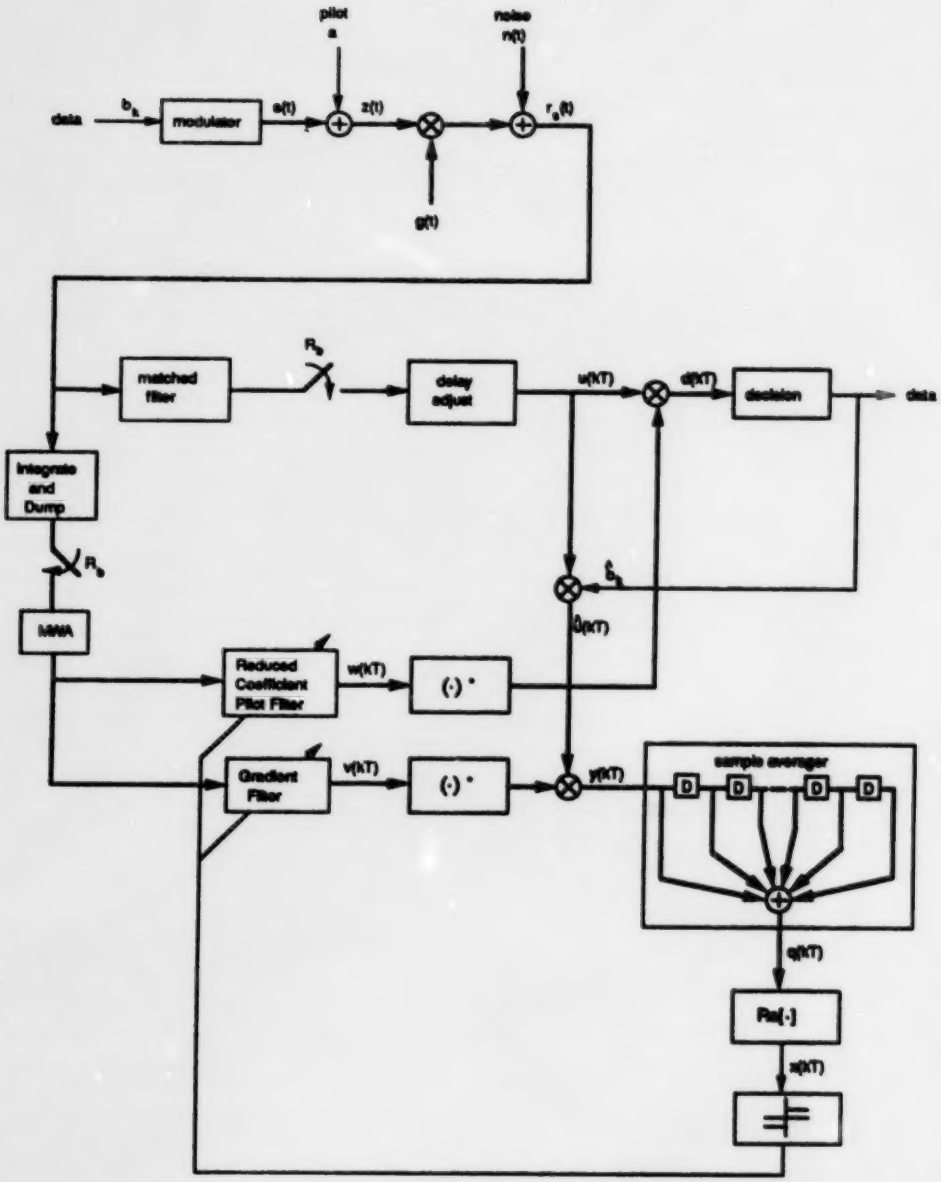

Figure 2 - Model of a Tone-aided Transmission System Using FSA for Pilot Recovery

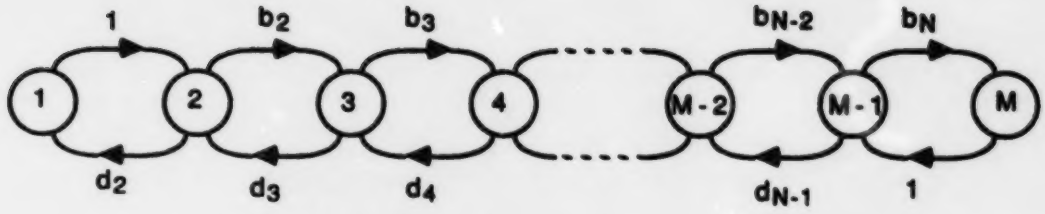

Figure 3 - Markov Chain Model of the Filter Switching Process

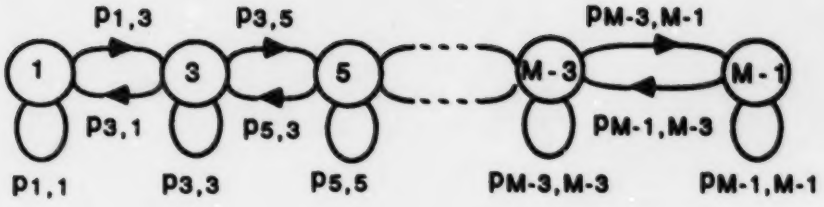

a. Odd State Chain

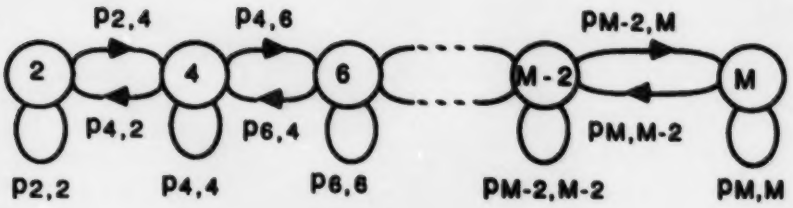

b. Even State Chain

Figure 4 - Dual Markov Chain Model of the Filter Switching Process for M even

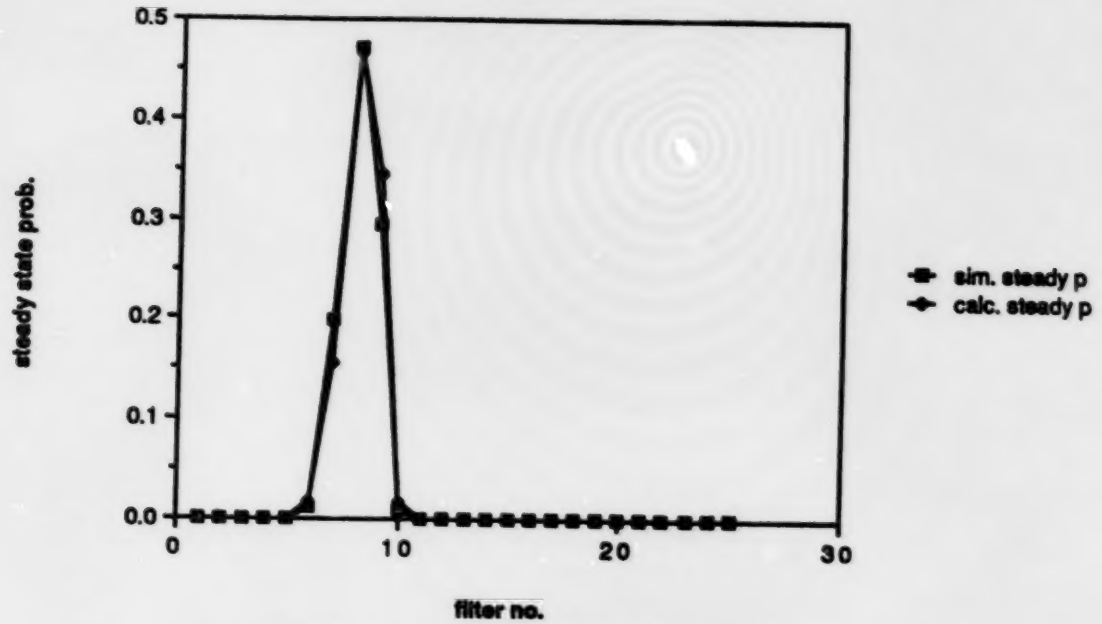

Figure 5 - Calculated vs. Simulated Steady State Probabilities

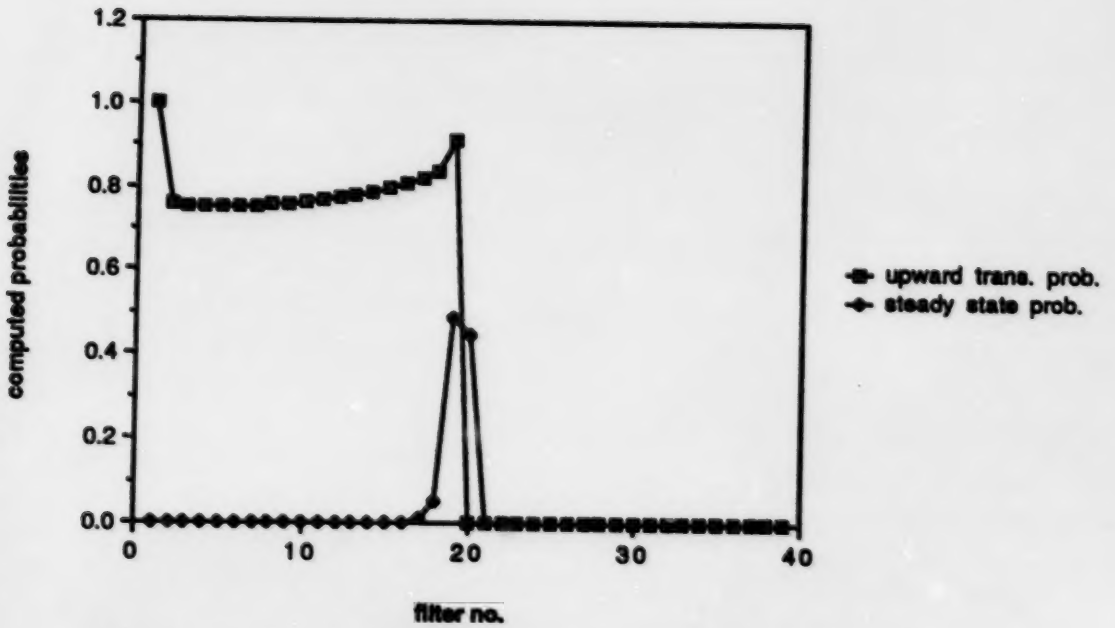

Figure 6 - Computed Probabilities for Filter Switching Algorithm using Ideal Rectangular Filters

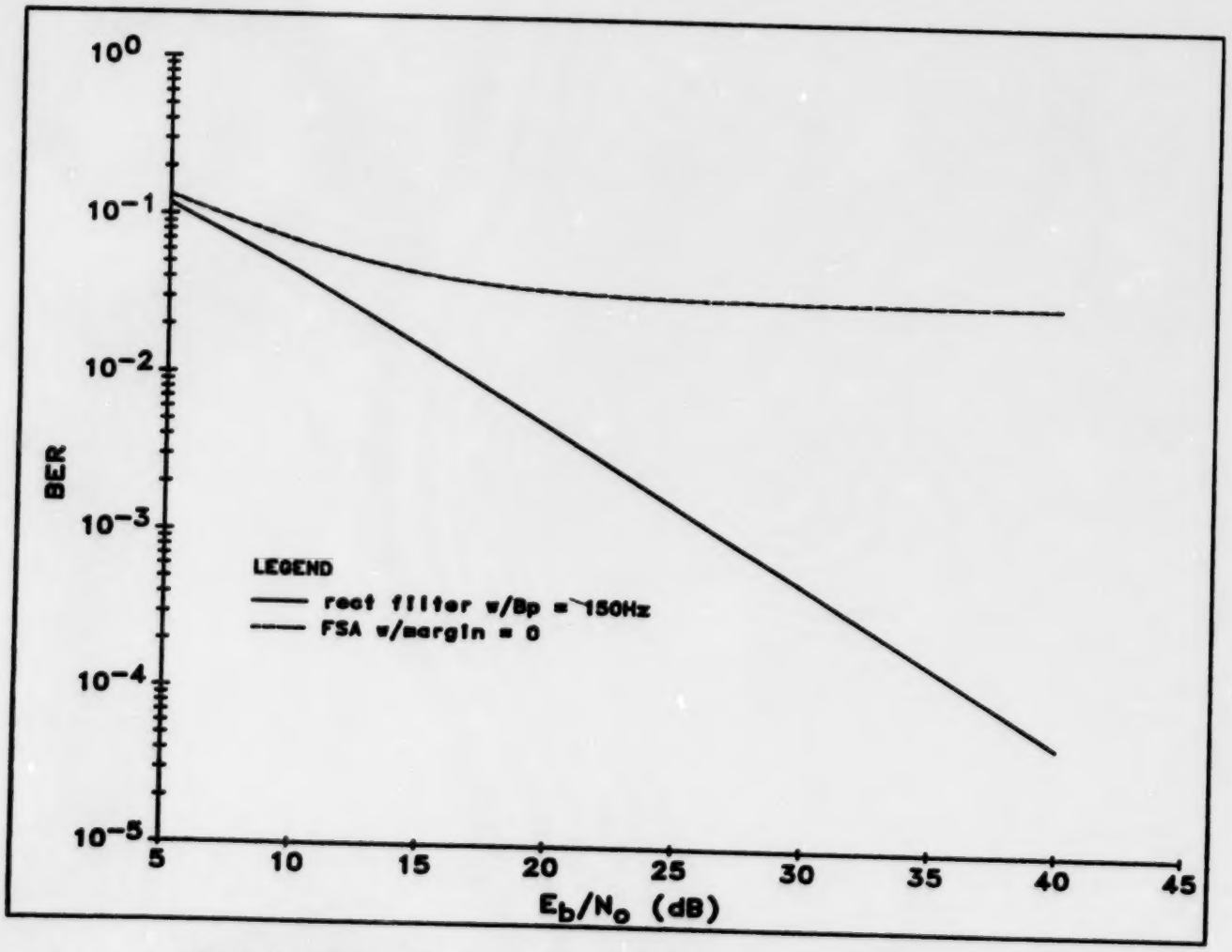

Figuire 7 - Average BER Performance of the FSA with no Step Margin

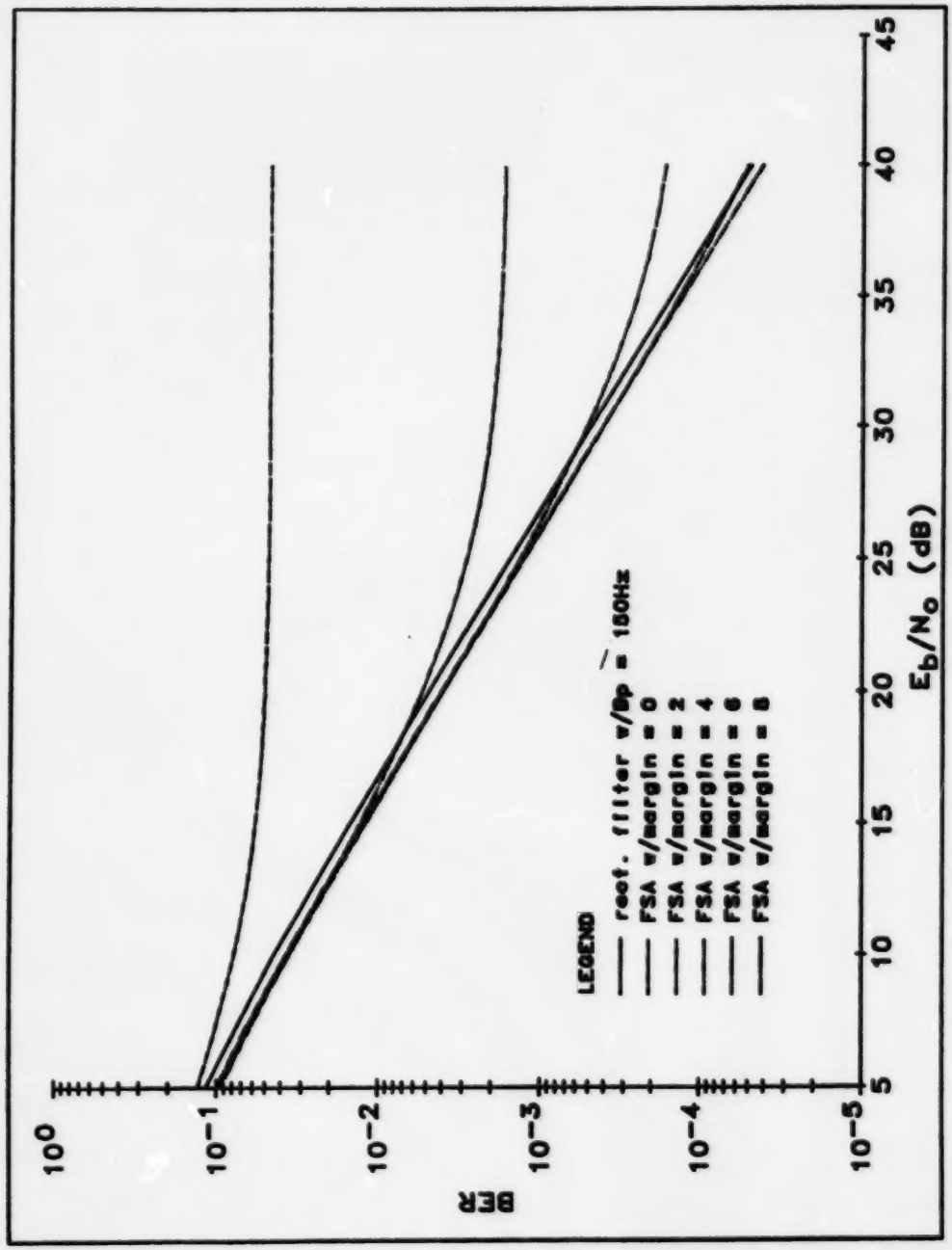

Figure 8 - Effect of Step Margin on the Average BER Performance of the FSA

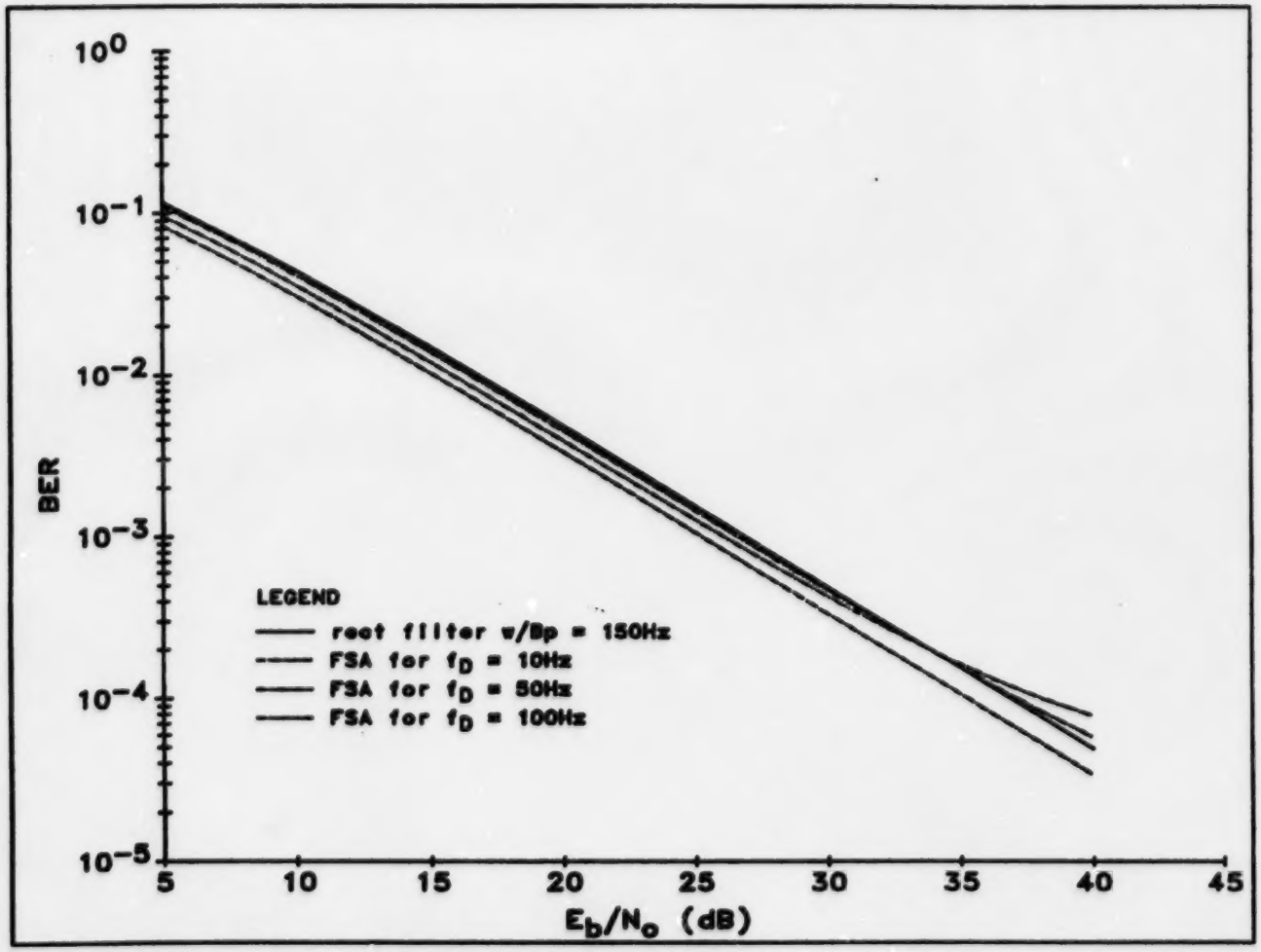

Figure 9 - Average BER Performance of the FSA at Various Doppler Frequencies

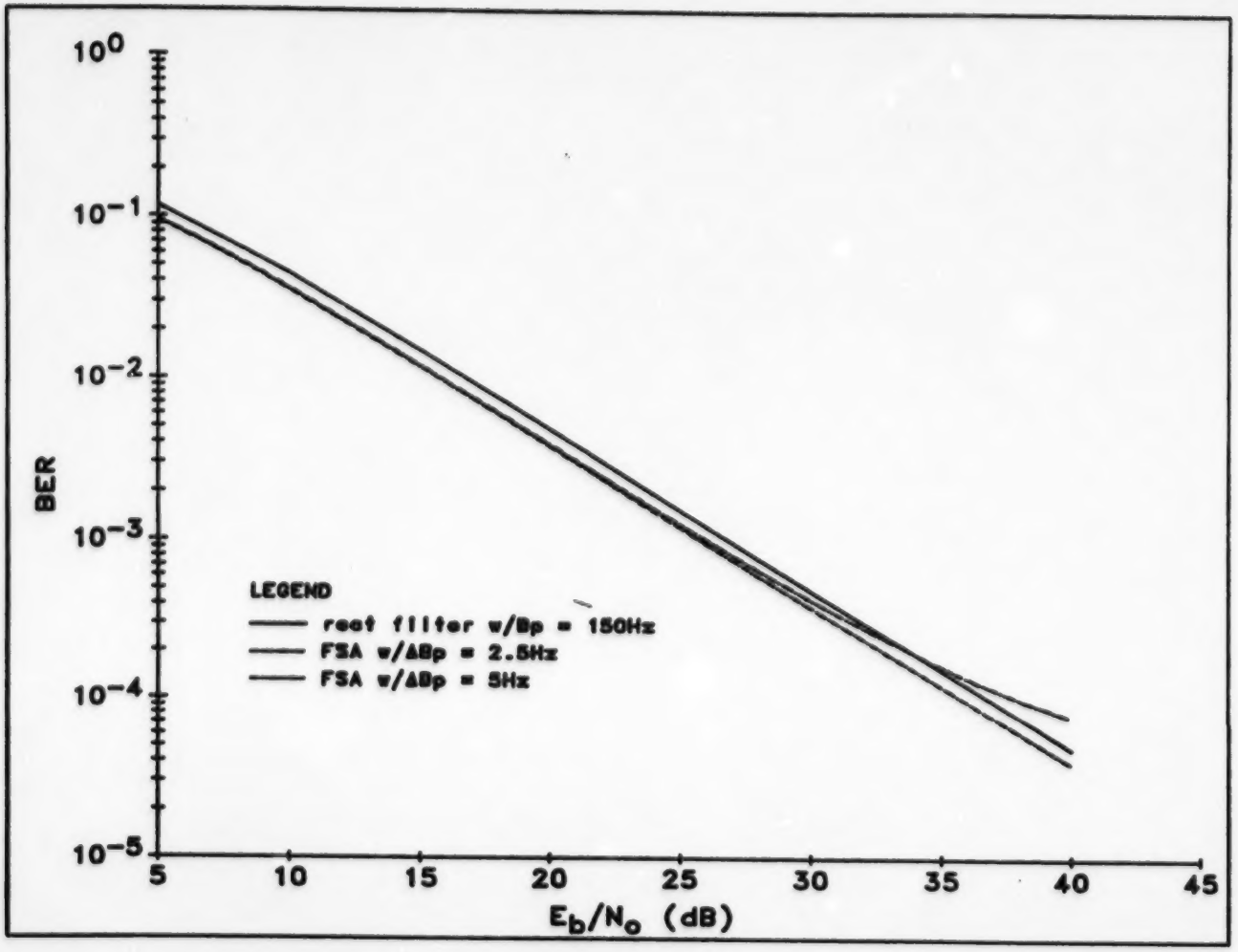

Figure 10 - Effect of Bandwidth Increment on the Average BER Performance of the FSA

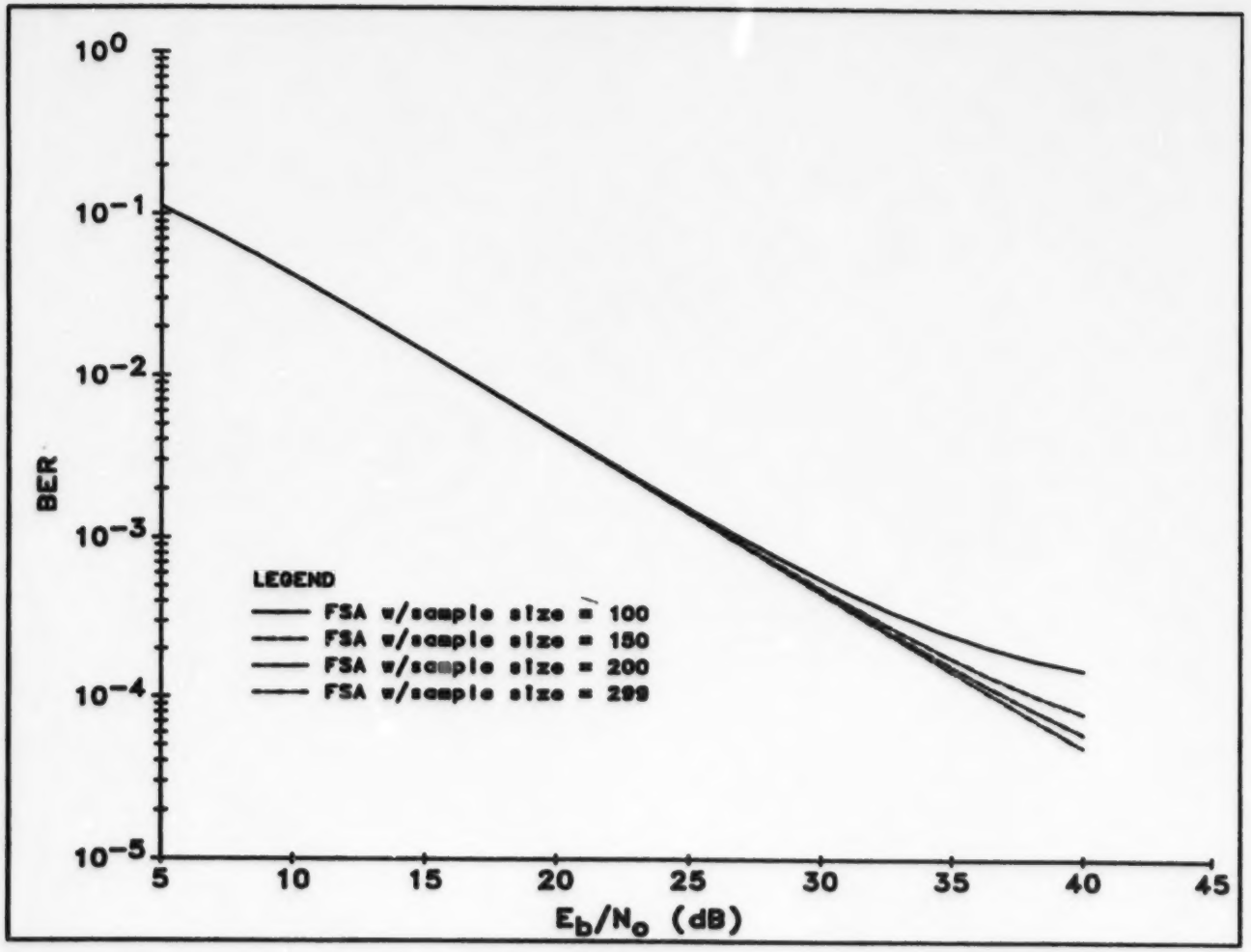

Figure 11- Effect of Cross-Correlation Sample Size on the Average BER Performance of the FSA

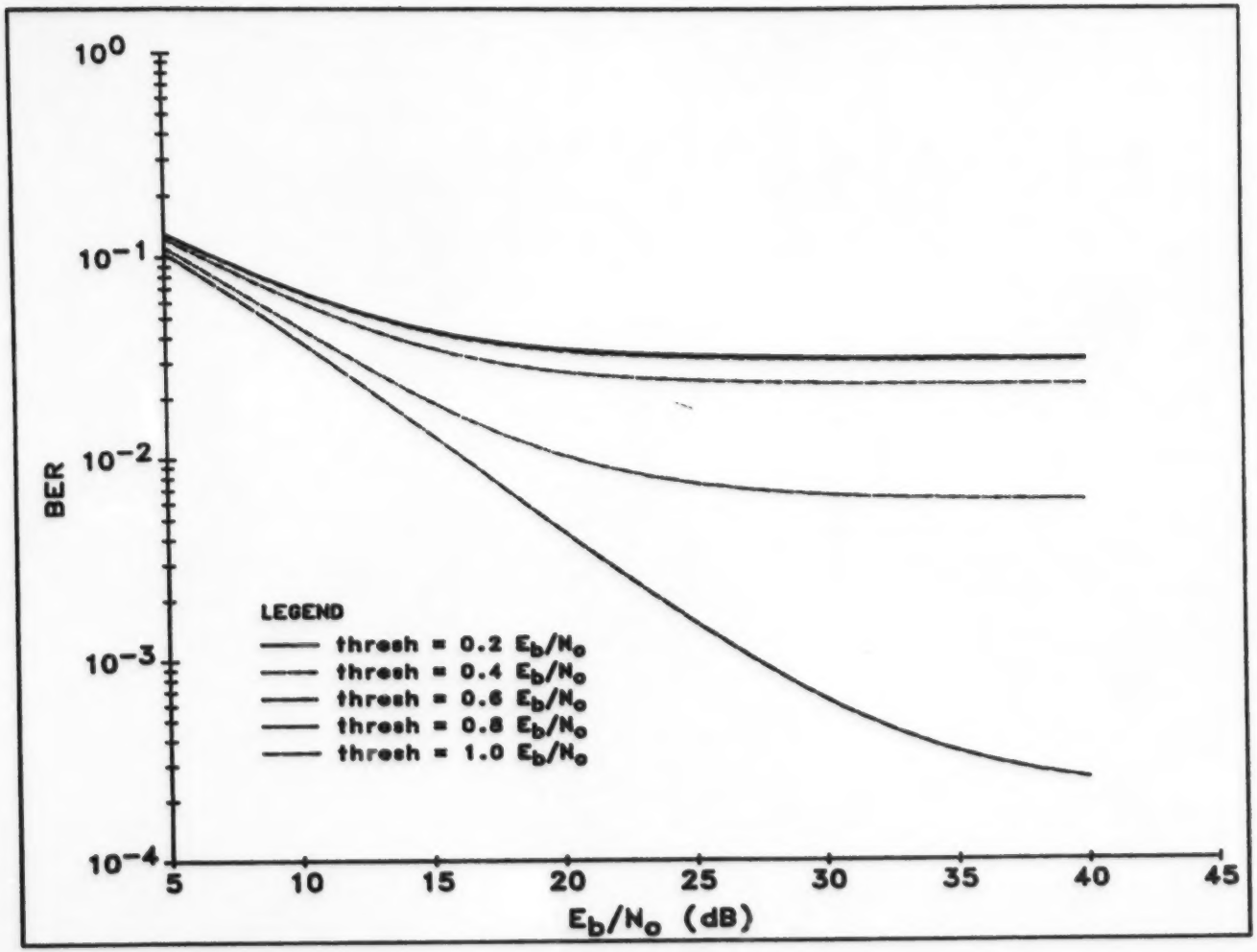

Figure 12 - Average BER Performance of the Dual Threshold FSA with Various Threshold Values

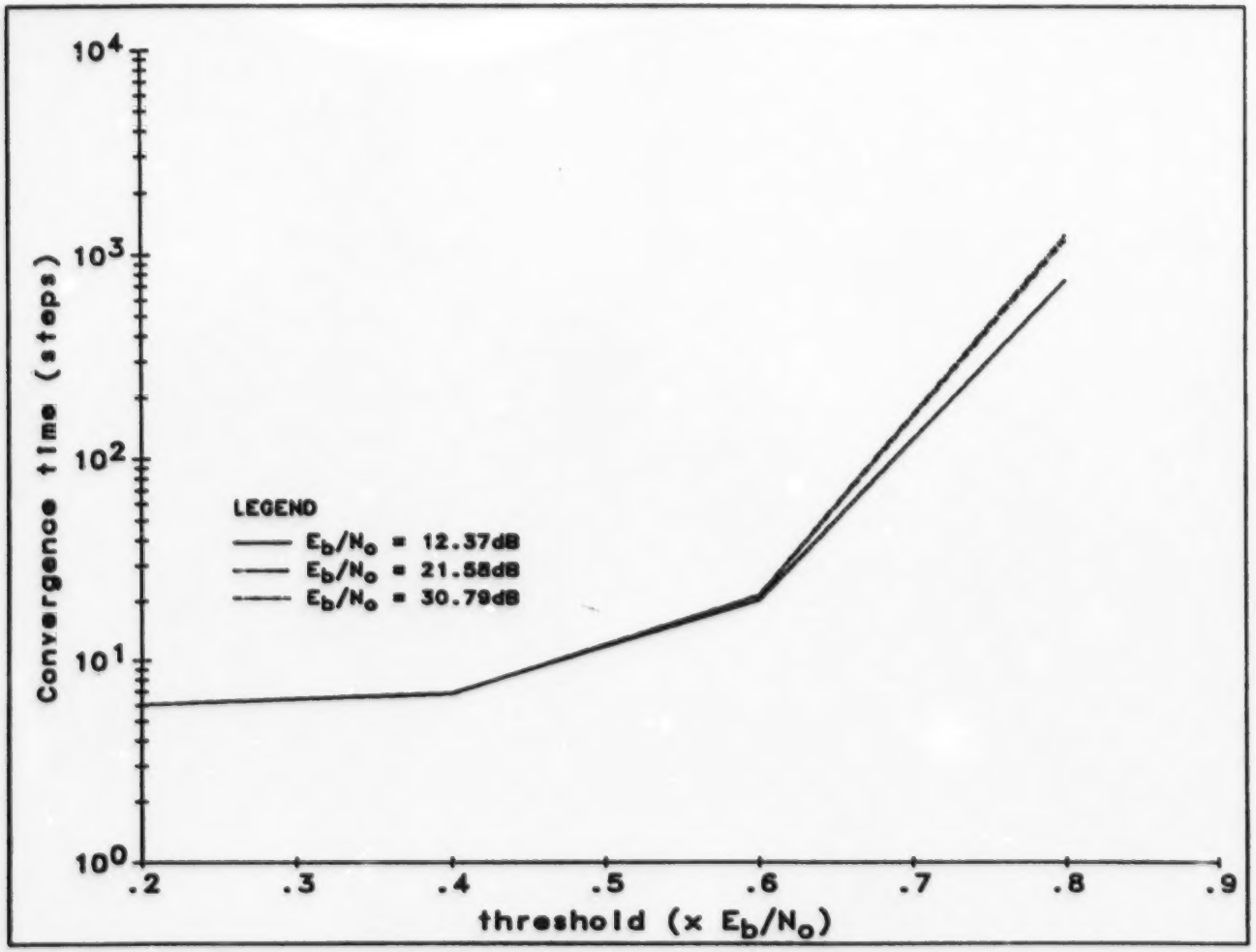

Figure 13 - Convergence Time of the Dual Threshold FSA with Various Threshold Values

Centre for Systems Science

• Simon Fraser University established the **Centre for Systems Science** as a provincial centre for advanced study. The objective of CSS is twofold: coordinate and combine advanced systems research at SFU, and encourage application of research results within industry in order to further the technological development of British Columbia.

• CSS has assembled three research groups to streamline its efforts. The orientation of these groups is as follows: intelligent systems, microelectronics, and computer and communications systems. Because of shared research interests, this latter group merges with LCCR (**Laboratory for Computer and Communications Research**) for the publication of technical reports.

• CSS's three groups involve over 80 skilled faculty researchers principally from SFU's Schools of Engineering Science and Computing Science, but also draw substantially on Mathematics, Physics, Geography, Philosophy, Linguistics, Psychology, Communication, and Kinesiology.